A Mathematical Model for Shear Stiffness and Dilation for Saw-Tooth Joints under CNL Conditions

Sujeet Bharti
Department of Mining Engineering, IIT Kharagpur, India

Rakesh Kumar
Department of Mining Engineering, IIT Kharagpur, India

Debasis Deb
Department of Mining Engineering, IIT Kharagpur, India

K. U. M. Rao
Department of Mining Engineering, IIT Kharagpur, India

ABSTRACT: An extensive direct shear test program has been conducted on regular saw-tooth artificial joint samples under constant normal load (CNL) conditions. The analysis of shear data reveals that shear stiffness ($k_{ss} = d\tau/du$) and dilation ($\psi = dv/du$), where τ and v are the shear stress and vertical displacement respectively, are not constants throughout the evolution of shear stress. Rather, it is clear that both the variables change non-linearly with shear displacements (u) and can be approximated by two-parameter hyperbolic function with respect to u. These parameters are estimated using regression analysis using the experimental data. From the functions $k_{ss}(u)$ and $\psi(u)$, a shear displacement exists at which the basic friction angle occurs. Also, it is found that this displacement occurs where contraction ends and dilation begins. Based on that, the dilatant behavior and evolution of peak shear strength can be described leading up to the determination of dilation angle at the peak stress.

Keywords: saw-tooth joint, direct shear test, mathematical model, shear stiffness, dilation.

1 INTRODUCTION

Joint can be defined as a line of break from geological formation along which there is no observable deformation (Muralha et al., 2014). In most of the literature, for regular saw-tooth shaped artificial samples under CNL boundary condition, shear behavior is mostly characterized by peak shear strength which depends on the normal load and dilation angle for a given basic friction angle (Budi et al., 2014; Haberfield & Johnston, 1994; Ladanyi & Archambault, 1969; Yang & Chiang, 2000; Zhu et al., 2019). A few studies have been conducted to understand the evolution of the mobilized friction angle while shearing, i.e. with shear displacement (Hoek & Brown, 1997; Barton, Bandis & Bakhtar, 1985; Bai et al., 2010). In other words, understanding the development of shear resistance of a joint surface with shear displacement may reveal the dilatant behavior as well as the variation of shear stiffness. In most of the applications, shear stiffness and dilation are considered to be the constant throughout the evolution of shear stress until the peak strength. From laboratory experiment results, it is clear that they are not constant rather vary nonlinearly with shear displacements even at the initial stages of loading. Therefore, from the relationships between shear stiffness/dilation angle and shear displacement, it may be possible to develop models of the peak shear strength and mobilized friction angle depending on shear displacement.

In order to investigate these phenomena and to develop relationships between shear stiffness/dilation with shear displacement, an extensive laboratory experiments on regular saw-tooth shaped artificial samples under CNL boundary condition are conducted in this paper. Several researchers have conducted studies on regular saw-tooth joint sample keeping the equal base length with certain asperity angle generally below 30^0 (Shrivastava & Rao, 2011; Li et al., 2014; Bahaaddini et al., 2016; Niktabar et al., 2016, 2017). From the above and vast literature, it is found that there exist research gaps on shear behavior of regular saw-tooth joint samples having variable base lengths i.e. varying the number of asperities in terms of developing a model of mobilized friction angle with respect to shear displacement. This paper mainly focused on CNL tests of regular saw tooth samples made of cement mortar for developing mathematical models of shear stiffness and dilation with respect to shear displacement and is discussed below.

2 EXPERIMENTAL STUDY AND RESULTS

The experimental work is carried out on cement mortar sample blocks of length 100 mm, width 100 mm and height 100 mm. The angle of regular saw-tooth asperities varied as 0^0, 10^0 and 20^0. A total of 70 tests was carried out under this study. Five normal stresses 0.303 MPa, 0.491 MPa, 0.679 MPa, 0.867 MPa and 1.055 MPa are defined as low normal stresses considering the criteria of $40 < \sigma_c/\sigma_n \leq 200$. The other hand five normal stresses 1.252 MPa, 2.183 MPa, 3.123 MPa, 4.063 MPa and 5.003 MPa are considered to be high normal stresses belonging to $1 \leq \sigma_c/\sigma_n \leq 40$. Here, σ_c = 44.67 MPa denotes the uniaxial compressive strength of the sample. For non-zero asperity samples, single (S), double (D) and quadruple (Q) asperities in a single sample are prepared by varying the base length of asperities. An automated 500 kN capacity servo-controlled direct shear machine with continuous data acquisition system is used for conducting all the CNL shear tests.

2.1 Shear behavior of 0^0, 10^0 and 20^0 regular saw-tooth samples

The reference samples having asperity angle, i = 0^0 exhibit increasing peak shear strength with normal stresses. Dilation angles remain near zero degree for all cases of normal stresses. Table 1 shows the peak shear strength versus normal stress data. The basic friction angles (ϕ_b) is found to be 38.2^0. The joint roughness coefficient (JRC) of all sets of surfaces are determined from Barton's envelop (Barton, 1973; Barton and Choubey, 1977) and also given in the Table 1. Figures 1(a), (b) and (c) plot the shear stress and vertical displacement versus shear displacement curves for 3 different

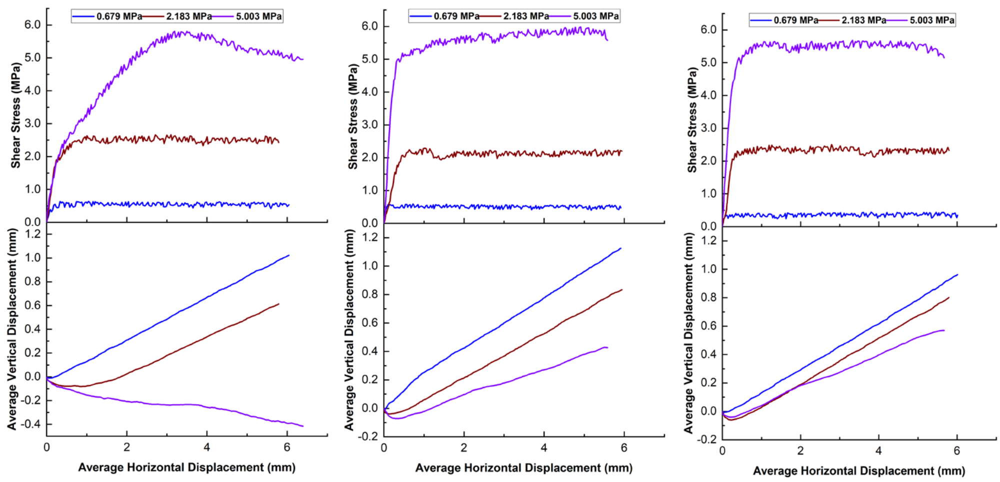

(a) Samples 10^0 –Single (b) Samples 10^0 –Double (c) Samples 10^0 –Quadruple

Figure 1. Shear stress and vertical displacement plots for representative 10^0 samples.

normal stresses viz. 0.679 MPa, 2.183 MPa and 5.003 MPa for single, double and quadruple samples having asperity angle 10^0 respectively. Note that these plots represent the trend of shear resistance provided by 10^0 asperity samples for the given normal stresses and the similar trend are observed for the rest of the normal stresses. The peak shear strengths are estimated for all the test results and are listed in Table 1. Figure 2(a) depicts the plots between peak shear strength versus normal stress and shows pseudo-linear relationship.

The key highlights of these results are (i) if $\sigma_n > 0.6$ MPa, a well-defined contraction zone occurs before the upper block shows dilatant behaviour, (ii) the contraction zone ($v < 0$ until $\psi = dv/du = 0$) is the manifestation of firm contact of the two blocks, and (iii) shear stiffness, $k_{ss} = d\tau/du$ is high at the beginning of the shearing process and gradually reduces with increasing shear displacement. The key highlights of 20^0 samples are (i) dilatant behavior is more prominent as compared to 10^0 samples, (ii) there is no significant improvement of shear strength from 10^0 samples, and (iii) several 20^0 single asperity samples show wavy nature of shear stiffness (k_{ss}) with shear displacement (u).

Table 1. Peak shear strength of 0^0, 10^0 and 20^0 samples (all values are in MPa).

Normal Stress (MPa)	Plane 0^0	τ_p (Single) 10^0 (JRC=10.08)	τ_p (Single) 20^0 (JRC =8.76)	τ_p (Double) 10^0 (JRC =8.66)	τ_p (Double) 20^0 (JRC =15.10)	τ_p (Quadruple) 10^0 (JRC =14.46)	τ_p (Quadruple) 20^0 (JRC =11.60)
0.303	0.152	0.107	0.061	0.115	0.122	0.041	0.064
0.491	0.219	0.425	0.332	0.302	0.471	0.194	0.324
0.679	0.495	0.638	0.740	0.592	0.828	0.443	0.864
0.867	0.579	0.843	1.080	0.773	1.215	0.737	0.971
1.055	0.757	1.134	1.480	0.974	1.471	0.941	1.262
1.252	1.039	1.712	2.016	1.329	2.170	1.637	1.888
2.183	1.801	2.667	3.604	2.291	3.594	2.507	2.712
3.123	2.511	3.859	5.339	3.608	5.092	3.637	4.100
4.063	3.059	4.983	6.627	4.604	5.762	4.647	5.114
5.003	4.016	5.810	7.003	5.990	6.883	5.684	6.462

2.2 *General behavior of shear stress versus shear displacement curves*

From the majority of $\tau - u$ curves for 10^0 and 20^0 asperity samples with different normal stresses, it is quite evident that k_{ss} and ψ are not constants for the range of shearing domain ($0 \leq u \leq u_p$), where u_p = shear displacement at peak shear strength as shown using an example in Figure 2(b). The

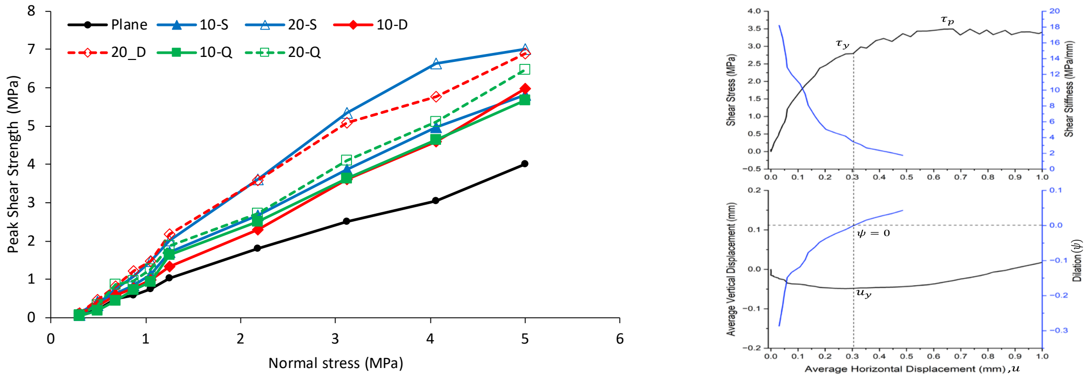

Figure 2. (a) Relationship between τ_p and σ_n (b) Yield shear stress, τ_y occurs at $\psi = 0$

shear stiffness is relatively high ranging over 20.0 MPa/mm. This signifies that the initial resistance provided by the sample is significant. However, once τ is reached the yielding limit (τ_y), the initial high resistance is lost and the shear stiffness drops significantly. Finally, it reaches to the peak shear stress τ_p at u_p generally ranging between 1 and 2 mm. Another significant observation is that the vertical movement of upper block (v) is downward or negative causing contraction, $dv/du < 0$, until $\tau \approx \tau_y$ (bottom graph of Figure 2(b)). Mostly, the sample dilates or $dv/du > 0$, once $u > u_y$. In all cases, it is found that dilation starts after yield stress (τ_y) is reached.

2.3 Mathematical models of mobilized shear stiffness and dilation

A computer program is written to estimate both k_{ss} and ψ as shown by representative samples in Figures 3(a) and (b) respectively. It can be clearly seen that k_{ss} values are very high ranging from 4.0 MPa/mm to 20.0 MPa/mm at the initial stage of loading signifying high frictional resistance at the joint surface. However, as u approaches to u_p, k_{ss} drops drastically signifying the loss of shear resistance.

On the contrary, the initial value of ψ is close to -0.5 to -0.8 mm/mm and can be as low as -1.0 mm/mm. However, it increases rapidly with u and crosses the 0 mark close to $u \approx u_y$. This ends the contraction period and marks as the beginning of dilation. Hence, for $u_y \leq u \leq u_p$, the evolution of shear stress is mainly dominated by the dilatant behaviour of the samples. In these samples, the maximum positive ψ is found to be around 0.15 to 0.2 mm/mm.

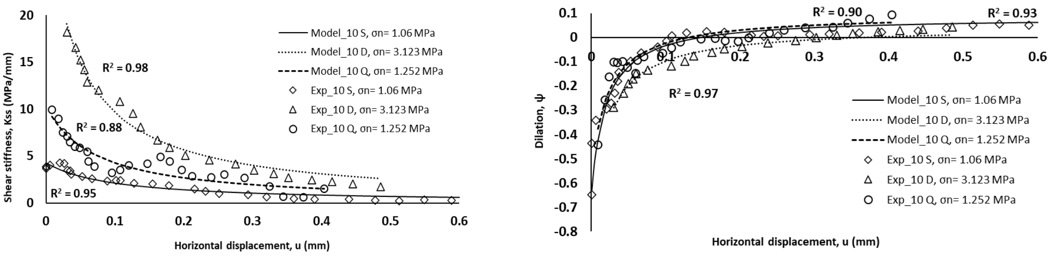

Figure 3. (a): Relationship between k_{ss} and u (b): Relationship between ψ and u.

From the above relationships, until $u \leq u_p$, k_{ss} can be expressed using two-parameters hyperbolic function as

$$k_{ss} = \frac{a}{u - b} \tag{1}$$

Where a and b are the constants to be determined from the $k_{ss} - u$ curve. The constant a may have a direct relation with k_{ss} and hence it reduces with the decreasing σ_n. The constant b is an offset parameter to u and the value of k_{ss} is sensitive to this parameter. Once the constants a and b are known, shear stress at any $u \leq u_p$ can be determined from the following equation as

$$\tau = a \ln\left(1 - \frac{u}{b}\right), \qquad u \leq u_p \tag{2}$$

The trend of ψ with u is also found to be hyperbolic but in this case it increases with increasing u. Again, since ψ ranges from negative to positive value, a parameter ψ_0 taken as the maximum value of ψ, is subtracted from the measured data and the regression analysis is performed. Therefore, the relationship resembles a hyperbolic function of the following form:

$$\psi = \frac{dv}{du} = \psi_0 + \frac{c}{u - d} \tag{3}$$

Where the constants c and d are to be determined by regression analysis. From equation 3, we can find that

$$v = \psi_0 u + c \ln\left(1 - \frac{u}{d}\right) \text{ and } u(\psi = 0) = d - \frac{c}{\psi_0} \tag{4}$$

2.4 *Mobilized friction angle and dilation angle at peak strength*

Based on the relationship mentioned in equations 2 and 3, τ_y can be estimated as

$$\tau_y = \tau(u_y) = \sigma_n \tan(\phi_y) \tag{5}$$

Where ϕ_y is the friction angle mobilized at $u = u_y$ or u at $\psi = 0$. Figure 4(a) plots τ_y versus σ_n for the representative samples comprising 10^0-S, 10^0-D and 10^0-Q, and 20^0-D and 20^0-Q samples. It is found that in the average sense, the friction angle at $u = u_y$ or u at $\psi = 0$, is about 37^0, which is very close to ϕ_b of 38^0. The range of ϕ_y may vary from 24 to 47 degrees based on the different values of σ_n. This result reveals an interesting hypothesis that in the average sense, the mobilized friction angle at the yielding shear displacement, i.e at u_y or u at $\psi = 0$, represents the basic friction angle. Similarly, the peak shear stress can be expressed as

$$\tau_p = \tau(u_p) = \sigma_n \tan(\phi_y + \phi_d) \tag{6}$$

Where ϕ_d is the additional angle mobilized due to dilatant behaviour of joint surface beyond $\psi = 0$. Needless to say, ϕ_d is dependent on σ_n and for higher value of σ_n, it may be completely suppressed. The mobilized dilation angle at the peak stress is then computed as

$$\tan \phi_d = \left(\frac{\tau_p - \tau_y}{\sigma_n + (\tau_p \tau_y / \sigma_n)}\right) \tag{7}$$

Figure 4(b) plots the dilation angle with σ_c/σ_n. For 10^0-S, 10^0-D and 10^0-Q samples, it is quite evident that dilation angle decreases with increasing σ_n. However, for other samples, it shows that the dilation angle may be over 25^0 for $\sigma_c/\sigma_n < 20$. This implies that if the asperity angle is high (20^0 in this case) dilation may occur irrespective of the value of normal stress.

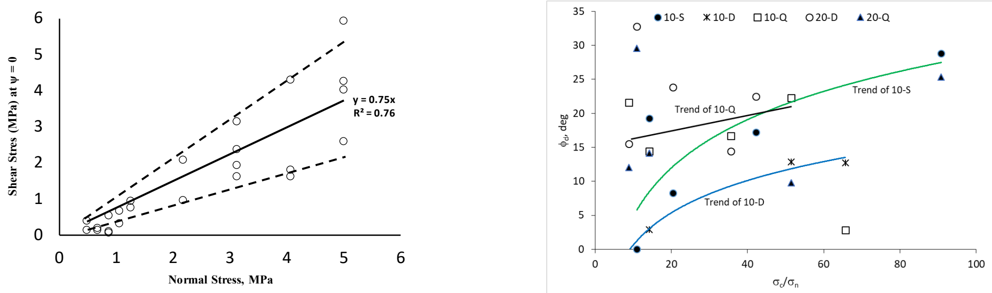

Figure 4. (a) Friction angle at τ_y or $\psi = 0$ (b) Relationship between dilation angle and σ_c/σ_n.

3 CONCLUSION

For regular saw-tooth samples, peak shear strength decreases by 2% to 60% from single to multiple asperity samples for asperity angle of 10^0 angle for low normal stress. For 20^0 asperity angle samples, the above decrease is less (2% to 25%). The average decrease in peak strength from 10^0-S samples to 10^0-D and 10^0-Q samples are 5% and 9% respectively, if the applied normal stress is high. However, for 20^0 asperities the average decrease in peak shear strength are found to be 2% and 17%

respectively for the same normal stresses. One of the objectives of this work is to investigate that both shear stiffness and dilation are not constants and are some functions of shear displacement. The study establishes the relationship as two-parameter hyperbolic function for both k_{ss} and ψ. It is also found that the shear displacement at zero dilation angle (u at $\psi = 0$) marks the yielding of the sample as well as the occurrence of basic friction angle. This is a remarkable coincidence since beyond this displacement ($u_y \leq u \leq u_p$), dilatant behaviour prevails. Based on the above, the development of shear stress ($\tau_p - \tau_y$) is due to the dilation of the joint. This work presents a mathematical framework for estimating basic friction angle and dilation angle using the k_{ss} and ψ functions. It is also established that shear stress τ is a logarithmic function of u and τ_p can be estimated as $\tau_p = \tau(u_p)$.

REFERENCES

Bahaaddini, M., Hagan, P. C., Mitra, R., & Khosravi, M. H. (2016). Experimental and numerical study of asperity degradation in the direct shear test. *Engineering Geology*, *204*. https://doi.org/10.1016/j.enggeo.2016.01.018

Bai, Z., Chen, Y., Zhou, C., Li, D., & Rong, G. (2010). Post-peak dilatancy and its evolution of hard rock fractures under normal and shear loads. *Yanshilixue Yu Gongcheng Xuebao/Chinese Journal of Rock Mechanics and Engineering*, *29*(SUPPL. 2).

Barton, N. (1973). Review of a new shear-strength criterion for rock joints. In *Engineering Geology* (Vol. 7, Issue 4, pp. 287–332). https://doi.org/10.1016/0013-7952(73)90013-6

Barton, N., Bandis, S., & Bakhtar, K. (1985). Strength, deformation and conductivity coupling of rock joints. *International Journal of Rock Mechanics and Mining Sciences And*, *22*(3), 121–140. https://doi.org/10.1016/0148-9062(85)93227-9

Barton, N., & Choubey, V. (1977). The shear strength of rock joints in theory and practice. *Rock Mechanics*, *10*(1–2), 1–54. https://doi.org/10.1007/BF01261801

Budi, G., Rao, K. U. M., & Deb, D. (2014). Laboratory modelling of rock joints under shear and constant normal loading. *International Journal of Research in Engineering and Technology*, *3*(4), 190–200.

Haberfield, C. M., & Johnston, I. W. (1994). A mechanistically-based model for rough rock joints. *International Journal of Rock Mechanics and Mining Sciences And*, *31*(4), 279–292. https://doi.org/10.1016/0148-9062(94)90898-2

Hoek, E., & Brown, E. T. (1997). Practical estimates of rock mass strength. *International Journal of Rock Mechanics and Mining Sciences & Geomechanics Abstracts*, *34*(8), 1165–1186. https://doi.org/10.1016/S0148-9062(97)00305-7

Ladanyi, B., & Archambault, G. (1969). Simulation of shear behavior of a jointed rock mass. *11th U.S. Symposium on Rock Mechanics, USRMS 1969*, *105*, 105–125.

Li, H. H., Wang, T. T., Huang, T. H., & Yang, Z. Y. (2014). Influences of shear rate on the mechanical behaviors of artificial rock joints with regular asperities. *ISRM International Symposium - 8th Asian Rock Mechanics Symposium, ARMS 2014*, 963–968.

Muralha, J., Grasselli, G., Tatone, B., Blümel, M., Chryssanthakis, P., & Yujing, J. (2014). ISRM suggested method for laboratory determination of the shear strength of rock joints: Revised version. *Rock Mechanics and Rock Engineering*, *47*(1). https://doi.org/10.1007/s00603-013-0519-z

Niktabar, S. M. M., Rao, K. S., & Shrivastava, A. K. (2016). Shear behaviour of regular and irregular rock joints under cyclic conditions. *3rd International Symposium on Mine Safety Science and Engineering*, 193–198.

Niktabar, S. M. M., Rao, K. S., & Shrivastava, A. K. (2017). Effect of rock joint roughness on its cyclic shear behavior. *Journal of Rock Mechanics and Geotechnical Engineering*, *9*(6), 1071–1084. https://doi.org/10.1016/j.jrmge.2017.09.001

Shrivastava, A. K., & Rao, K. S. (2011). Shear behaviour of non planar rock joints. *14th Asian Regional Conference on Soil Mechanics and Geotechnical Engineering*. https://doi.org/10.13140/2.1.2357.2486

Yang, Z. ., & Chiang, D. . (2000). An experimental study on the progressive shear behavior of rock joints with tooth-shaped asperities. *International Journal of Rock Mechanics and Mining Sciences*, *37*(8), 1247–1259. https://doi.org/10.1016/S1365-1609(00)00055-1

Zhu, J. B., Li, H., & Deng, J. H. (2019). A One-Dimensional Elastoplastic Model for Capturing the Nonlinear Shear Behaviour of Joints with Triangular Asperities Based on Direct Shear Tests. *Rock Mechanics and Rock Engineering*, *52*(6), 1671–1687. https://doi.org/10.1007/s00603-018-1674-z